

# Atomtronic multi-terminal Aharonov-Bohm interferometer

Jonathan Wei Zhong Lau,<sup>1,\*</sup> Koon Siang Gan,<sup>1</sup> Rainer Dumke,<sup>1,2</sup>  
Luigi Amico,<sup>1,3,4,5,†</sup> Leong-Chuan Kwek,<sup>1,6,7,8</sup> and Tobias Haug<sup>9,‡</sup>

<sup>1</sup>Centre for Quantum Technologies, National University of Singapore 117543, Singapore

<sup>2</sup>School of Physical and Mathematical Sciences, Nanyang Technological University 637371, Singapore

<sup>3</sup>Quantum Research Centre, Technology Innovation Institute, Abu Dhabi, UAE

<sup>4</sup>INFN-Sezione di Catania, Via S. Sofia 64, 95127 Catania, Italy

<sup>5</sup>LANEF 'Chaire d'excellence', Université Grenoble-Alpes & CNRS, F-38000 Grenoble, France

<sup>6</sup>MajuLab, CNRS-UNS-NUS-NTU International Joint Research Unit, UMI 3654, Singapore

<sup>7</sup>National Institute of Education, Nanyang Technological University, 1 Nanyang Walk, Singapore 637616

<sup>8</sup>School of Electrical and Electronic Engineering Block S2.1, 50 Nanyang Avenue, Singapore 639798

<sup>9</sup>QOLS, Blackett Laboratory, Imperial College London SW7 2AZ, UK

(Dated: May 4, 2022)

Manipulating the flow of cold atoms promises practical devices for quantum technologies. Here, we study a three-terminal atomic ring circuit pierced by a synthetic magnetic flux as a powerful multi-functional device. The flux controls the transport through the ring via the Aharonov-Bohm effect. The device can measure the flux in-situ via a flux-induced transition of the reflections from negative Andreev-like to positive. By exciting the system we break an emergent symmetry of the flux. This allows us to direct the atomic current into specific output ports via the flux, realizing a flexible non-reciprocal switch to connect multiple atomic systems together. Our system allows us to study the time-dependent Aharonov-Bohm effect in a controllable manner. While the Aharonov-Bohm effect for time-dependent magnetic fields and electrons is an open problem, for cold atoms we observe a clear periodic modulation of the current with a time-dependent synthetic flux. This allows us to realize an atomic frequency generator as well as a converter between direct and alternating current. Our results can be directly implemented in experiments to create novel quantum technological devices.

Precise control over quantum systems has led to the rapid development of quantum technologies for applications in quantum simulation, quantum communication and metrology. These fields are fundamental to Atomtronics [1], the emerging quantum technology of propagating cold atoms within matter-wave circuits [1–6]. Inspired by electronics, Atomtronics makes use of the coherence and control over cold atoms to realize novel and practical quantum devices.

Simple atomtronic circuits with Bose-Einstein condensates or degenerate fermions in ring-shaped potentials have been studied extensively in theory and experiments [6–8]. These studies enable cold atom rotation sensors with enhanced performance [9–13]. The recent progress in light-sculpting techniques enable the development of atomtronic devices with unprecedented control over the system geometry and parameters [14–17]. This opens up the development of integrated matter-wave circuits that combine cold atom circuits into a single atomtronic device capable of multiple functionalities. These integrated circuits could connect multiple atomic systems, act a precise rotation sensor and help to understand quantum transport phenomena [15].

The fundamentals of cold atom transport have been studied experimentally [18–25]. Analogues of one-dimensional mesoscopic conductors have been explored [26–30] with transport now possible over macroscopic distances [31]. In particular, Bose-Einstein condensates in ring shaped potentials [32–34] and Y-shaped

junctions [15, 35, 36] promise to realize practical devices. Such systems can exhibit superfluid current flows [37–40] and realize effective two-level dynamics for an Atomtronic qubit [41, 42].

In such ring-shaped geometries, a versatile technique to control transport relies on the Aharonov-Bohm effect where the magnetic flux changes the interference of matter [43]. The Aharonov-Bohm effect has many interesting implications for many-body physics [44–47] and quantum foundations [48, 49]. In mesoscopic electronic rings, the Aharonov-Bohm effect controls the conductance [50–53]. An open theoretical and experimental question is whether a time-dependent magnetic field produces an Aharonov-Bohm effect [54–57]. Cold atoms allow for the exploration of the Aharonov-Bohm effect in a controlled setting that is difficult to reach with other systems. The magnetic field is mimicked by a synthetic flux generated by driving the system in time [58–61] or via rotation [38, 62, 63]. With the Aharonov-Bohm effect one can control the transport of atoms through cold atom systems [34–36].

Here, we investigate a three-terminal ring controlled by the Aharonov-Bohm flux as a powerful multi-functional atomtronic device. The dynamics close to the ground state features a flux-induced transition. We find that density waves change from negative Andreev-like to positive due to the Aharonov-Bohm effect, which can be used for rotation sensing. The dynamics far from the ground state breaks the symmetry between the two drains. This

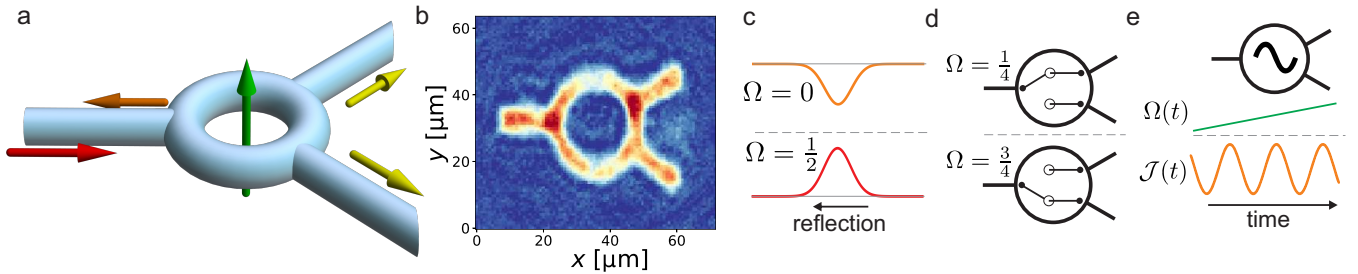


FIG. 1. **a)** Three-terminal Aharonov-Bohm circuit with source lead (left) attached to a ring with two drain leads (right). A synthetic Aharonov-Bohm flux  $\Omega$  is applied to the ring, which controls the current flowing through the ring. **b)** Experimental demonstration of the setup with a Bose-Einstein condensate.  $6 \cdot 10^4$  atoms are cooled to 50 nK by atom evaporation into an optical potential created by a digital micromirror device. We show the in-situ atomic density measured with absorption imaging. The device has various applications. **c)** Reflection of density waves changes from negative Andreev-like to positive with  $\Omega$ , which can be used for rotation sensing. **d)** Directional switch of the current to one of the output terminals by adjusting  $\Omega$ . **e)** Driving of  $\Omega(t)$  in time results in a sinusoidal output current, realizing an atomic frequency generator or a DC/AC converter.

allows us to control the output terminal of the current to realize a non-reciprocal switch. Finally, a constant acceleration of the synthetic flux leads to a time-dependent Aharonov-Bohm effect with a periodic modulation of transport. Remarkably, this effect can be applied for an atomic frequency generator or a converter between direct current (DC) and alternating current (AC).

*Model.*— A sketch of the three-terminal ring pierced by flux  $\Omega$  is shown in Fig. 1a. We experimentally demonstrate the setup with a Bose-Einstein condensate within an optical potential in Fig. 1b (see SM D for details). In the following, we simulate our system numerically by modeling it with the Bose-Hubbard model and divide the system into the source lead, two drain leads and the ring with  $L$  sites. The source lead  $s$  and the two drains  $b, c$  are connected to the ring in a symmetric manner with  $x_s = 1$ ,  $x_b = L/3$  and  $x_c = 2L/3$ . The system Hamiltonian  $H = H_r + H_\ell + H_{r\ell}$  is given by

$$H_r = \sum_{j=1}^L \left[ \frac{U}{2} \hat{n}_j (\hat{n}_j - 1) - J(e^{-i2\pi\Omega(t)/L} \hat{a}_{j+1}^\dagger \hat{a}_j + H.C.) \right]$$

$$H_{r\ell} = -K \sum_{\alpha=\{b,c,s\}} \left( \hat{a}_1^\dagger \hat{a}_{x_\alpha} + H.C. \right) \quad (1)$$

$$H_\ell = \sum_{\alpha=\{b,c,s\}} \sum_{j=1}^{L_\alpha} \left[ \frac{U_\alpha}{2} \hat{n}_j^\alpha (\hat{n}_j^\alpha - 1) - J_\alpha (\hat{a}_{j+1}^\dagger \hat{a}_j + H.C.) \right]$$

where  $\hat{a}_j (\hat{a}_j^\dagger)$  is the bosonic annihilation (creation) operator at site  $j$  on the ring, and  $\hat{n}_j = \hat{a}_j^\dagger \hat{a}_j$  is the corresponding number operator. We impose periodic boundary conditions in the ring with  $\hat{a}_{L+1} = \hat{a}_1$ .  $\Omega(t)$  represents the total flux through the ring which can be dependent on time  $t$ . For time-independent  $\Omega$ , the properties of the system are periodic with  $\Omega \rightarrow \Omega + k$ ,  $k$  being integer.  $J$  is the intra-ring coupling strength and  $U$  the interaction strength of the ring.  $\hat{a}_j$  is the annihilation operator,  $\hat{n}_j^\alpha$  the number operator,  $L_\alpha$  the number of sites,  $U_\alpha$  the

interaction strength and  $J_\alpha$  the intra-reservoir couplings for the source and drains with  $\alpha \in \{s, b, c\}$ . The current operator between lead  $\alpha$  and ring is given by

$$J_\alpha = -iK(\hat{a}_1^\dagger \hat{a}_{x_\alpha} - H.C.). \quad (2)$$

*Dynamics close to ground state.*— First, we study the dynamics close to the ground state as function of flux  $\Omega$ . We add a perturbation Hamiltonian with the local potential acting on the sites of the source Hamiltonian  $H_e = -\epsilon_s \sum_{j=1}^{L_s} \exp[-(j-D)^2/2\sigma^2] \hat{n}_j^s$  with  $D = L_s/2$ ,  $\sigma = 2$  and  $\epsilon_s = 0.3$ . We first prepare the ground state of the Hamiltonian  $H + H_e$ . The ground state has a slightly raised density in the source on the sites where  $H_e$  is acting on. At  $t > 0$  we switch off  $H_e$  and evolve the system only with Hamiltonian  $H$ . The raised density starts to move in both positive and negative direction as a density wave. We investigate the change in density  $\Delta n(t) = \langle n(t) \rangle - n_0$  in time, where  $n_0$  is the average density of the total system. The dynamics is calculated using matrix product states with the ITensor library [64]. In Fig. 2a we show the dynamics of  $\Delta n(t)$  for  $\Omega = \frac{1}{4} + k$ ,  $k$  being integer, as function of time  $t$  and the sites of source, ring and drain (see SM B for other values of  $\Omega$ ). We find that the forward propagating density wave moves from the source to the ring, then is transmitted into the drains as well as reflected back to the source. For any value of  $\Omega$  we find that the transmission into drain 1 and drain 2 is nearly the same. The magnitude of the current  $J$  into the first drain is shown in Fig. 2b. The current is maximal for  $\Omega = k$  and minimal for  $\Omega = \frac{1}{2} + k$ . We find nearly the same current for  $\Omega = \frac{1}{4} + k$  and  $\Omega = \frac{3}{4} + k$ , which is the result of an emergent reflection symmetry  $\Omega \rightarrow -\Omega$ . We show the density  $\Delta n$  at a fixed site in source and drain in Fig. 2c. We find that the reflection into the source at  $t = 27$  changes in nature with  $\Omega$ . For  $\Omega = k$  we find a clear negative reflection, which is the hallmark of Andreev reflections. With increasing  $\Omega$ , the Andreev reflections turn into positive reflections.

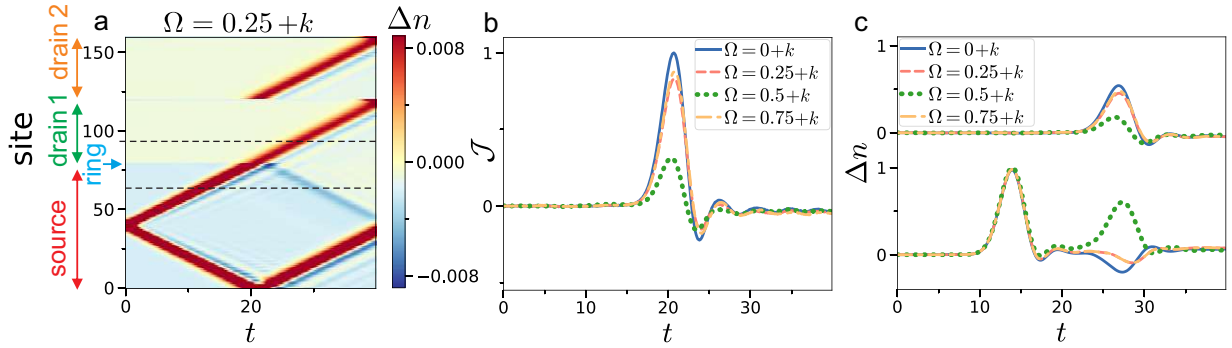


FIG. 2. Dynamics of density wave in three-terminal device. **a)** Change of density relative to average density  $\Delta n(t) = \langle n(t) \rangle - n_0$  as function of time and sites of source, ring, drain 1 and 2 for  $\Omega = \frac{1}{4} + k$ , where  $k$  is an integer. The density wave starts in source, and moves through ring into drains. Note that the dynamics in both drains is nearly symmetric for all values of flux. **b)** Current  $J$  into the first drain against time and  $\Omega$ . **c)**  $\Delta n$  in source (bottom) and first drain (top) measured at positions shown as dashed lines in a). The reflected density wave appears at  $t = 26$  in the bottom curve. We have hard-core bosons with  $J = 1$ ,  $K = 0.5$ ,  $L = 3$ ,  $L_s = 80$ ,  $L_b = L_c = 40$ .

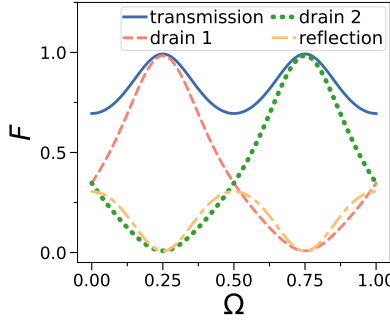


FIG. 3. Landauer formalism for three-terminal ring device for non-interacting bosons. We show the total transmission and reflection of the source, as well as the transmission into drain 1 and 2 as function of flux  $\Omega$ .

*Dynamics far from ground state.*— Now, we investigate the dynamics when the system is far from the ground state. We assume that the ring and drains are initially empty. Then, the ring is coupled to the source lead filled with atoms, which injects atoms into the ring. In the limit of zero interaction  $U = 0$  we describe the dynamics with the Landauer formalism as explained in SM A. The resulting transmission and reflection of the system is shown in Fig.3. In contrast to the dynamics close to the ground state, the transmission into drain 1 differs from drain 2 as function of  $\Omega$ . As a result, for  $\Omega = \frac{1}{4}$  we have unit transmission into drain 1, and zero transmission into drain 2. For  $\Omega = \frac{3}{4}$  the dynamics of the drains is interchanged, with maximal transmission into drain 2 and zero into drain 1. Thus, we can direct the all of the current either into drain 1 or drain 2, realizing a perfect non-reciprocal switch with zero back-reflection.

Next, we investigate the limit of strong interaction with hard-core bosons, where each site occupies at most one boson. We further simplify the source and drain leads

by tracing out all of their sites except the very first one coupled to the ring ( $\hat{s}_1$ ,  $\hat{b}_1$  and  $\hat{c}_1$ ). The effect of the reservoirs on the reduced density matrix  $\rho$  within the Born-Markov approximation is encapsulated by Lindblad operators  $L_m$  [35, 65]

$$\frac{\partial \rho}{\partial t} = -\frac{i}{\hbar} [H, \rho] - \frac{1}{2} \sum_m \{ L_m^\dagger L_m, \rho \} + \sum_m L_m \rho L_m^\dagger \quad (3)$$

with the dissipators  $L_1 = B_s \hat{s}_1^\dagger$ ,  $L_2 = B_b \hat{b}_1$  and  $L_3 = B_c \hat{c}_1$ .  $L_1$  describes bosons entering the system at the source site, and  $L_2$ ,  $L_3$  atoms leaving to the respective drains. We solve for the steady-state  $\rho_{ss}$  via  $\partial \rho_{ss} / \partial t = 0$  [66].

In Fig.4a and b we show the steady-state current through source and drains as function of flux  $\Omega$ . The current in drain 1 and 2 varies strongly with  $\Omega$ , allowing for directional control into either drain. For the source current, we find for  $J = 0.5$  in Fig.4a no variation with  $\Omega$ , whereas for  $J = 1$  the current in source varies strongly (Fig.4b). In Fig.4c, we show the average of the current over  $\Omega$  as function of intra-ring coupling  $J$ . We show the mean drain current  $\langle J_{\text{drain}} \rangle$ , the amplitude of the source current  $\Delta J_{\text{source}} = J_{\text{source}}^{\text{max}} - J_{\text{source}}^{\text{min}}$  and the maximal difference between the two drain currents  $\Delta J_{\text{drains}} = \max_{\Omega} (|J_{\text{drain 1}}(\Omega) - J_{\text{drain 2}}(\Omega)|)$ . We find a transition from  $\Delta J_{\text{source}} \approx 0$  to  $\Delta J_{\text{source}} > 0$  for  $J > 0.5$ . Further, the amplitude and mean value of the drain current shows a peak at the transition  $J \approx 0.5$ .

*Time-dependent flux.*— Now, the flux  $\Omega(t) = t/T$  is linearly increased in time with a period  $T$ . This could be achieved by a constant acceleration of the rotation affecting the ring. As a result, the current undergoes a periodic modulation. We study the current as function of driving period  $T$  in Fig.5. For  $t > 0$ , we inject atoms via the source into initially empty ring and drains. We show the dynamics for  $T = 1$  in Fig.5a and  $T = 2.8$  in Fig.5b. For

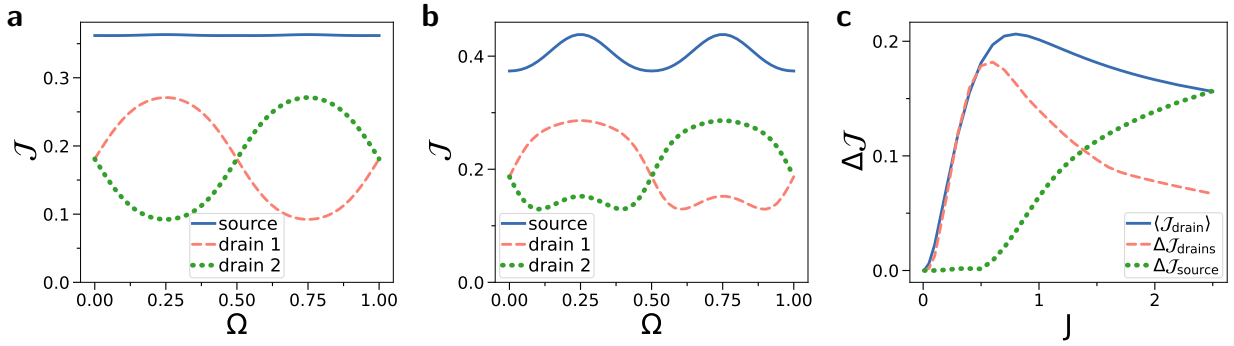


FIG. 4. Steady-state current  $\mathcal{J}$  as function of flux  $\Omega$  for **a**)  $J = 0.5$  **b**)  $J = 1$ . **c**) Mean value of drain current  $\langle \mathcal{J}_{\text{drain}} \rangle$  taken over  $\Omega$ , amplitude of source current  $\Delta \mathcal{J}_{\text{source}} = \mathcal{J}_{\text{source}}^{\text{max}} - \mathcal{J}_{\text{source}}^{\text{min}}$  as well as maximal difference between drain 1 and drain 2 current  $\Delta \mathcal{J}_{\text{drains}} = \max_{\Omega} (|\mathcal{J}_{\text{drain 1}}(\Omega) - \mathcal{J}_{\text{drain 2}}(\Omega)|)$  as function of intra-ring coupling  $J$ . We set  $L = 3$ ,  $K = 1$  and  $B_s = B_d = 1$ .

all  $T$ , the current undergoes an initial transient until it settles into a periodic oscillation with a period  $f = 1/T$ . For small  $T = 1$  in Fig. 5a, we find only small oscillations as the driving is faster than the system dynamics. For very large  $T \ll 1$  the driving is much slower than the system dynamics, and the current describes follows the instantaneous steady state  $\rho_{\text{ss}}(\Omega)$  (see SM C). For  $T = 2.8$  in Fig. 5b, we find large sinusoidal oscillations where the drain current is shifted by  $T/2$ , i.e. when one of the drains has minimal current, the other drain has maximal current. The drain current oscillates between close to 0 and the total current incoming via the source. This device realizes an atomic DC/AC converter where a constant source current is converted into an alternating current. For an optimal conversion, we want the amplitude of the drain current oscillation to be as close as possible to the incoming source current.

We investigate the conversion efficiency  $C = \Delta \mathcal{J}_{\text{drain}} / \langle \mathcal{J}_{\text{source}} \rangle$  of the DC/AC converter as function of  $T$  and  $J$  in Fig. 5c. We define the drain current amplitude  $\Delta \mathcal{J}_{\text{drain}} = \max_{t/T \gg 1} \mathcal{J}_{\text{drain}}(t) - \min_{t/T \gg 1} \mathcal{J}_{\text{drain}}(t)$  and the mean source current  $\langle \mathcal{J}_{\text{source}} \rangle = \text{mean}_{t/T \gg 1} \mathcal{J}_{\text{source}}(t)$ , where we ignore the initial transient dynamics and take the maximum over the long-time behavior  $t/T \gg 1$ . For  $C = 1$  the drain oscillation matches the source current, implying that the all of the source current is converted from DC to AC. We find that  $\Delta \mathcal{J} / \langle \mathcal{J}_{\text{source}} \rangle$  increases sharply with  $T$  and reaches a peak around  $T = 2.8$  for  $J \leq 0.5$ , then decreases. For  $J = 1$  we observe pronounced peaks and dips akin to resonances. For large  $T$ , the current follows the instantaneous steady state as function of  $\Omega$  and converges to the current amplitude of the steady state. We find maximal DC/AC conversion with  $C \approx 0.88$  for  $J = 0.5$  and  $T = 2.8$ .

*Discussion.*— The Aharonov-Bohm flux controls the dynamics of cold atoms in a three-terminal ring circuit to realize a multi-functional atomtronic device.

For the dynamics close to the ground state, we trans-

port density waves through the device. The flux controls the conductance, yielding a maximal current for  $\Omega = 0$  and minimal for  $\Omega = \frac{1}{2}$ . We observe negative Andreev-like reflection which have been observed in bosonic Y-junctions [35] and at interfaces between different interactions strengths [67, 68]. *Our setup controls the type of reflection with flux  $\Omega$ , changing from negative Andreev-like to positive.* This change in sign could be used to measure the flux for rotation sensing, as by carefully measuring the properties of the reflected density wave, the value of flux can be subsequently obtained, with positive reflection indicating a value of flux close to half-integer. In contrast to most atomic rotation sensor which need time-of-flight measurements, in our setup the flux can be read out in-situ which could be done in a non-destructive manner. We note that for any value of flux both drains have symmetric currents. We believe the phase of the Bose-Einstein condensate interacting with the flux induces this symmetry.

We find a different behavior for the dynamics far from the ground state, where atoms flow from source into an empty ring and drains. Both non-interacting (Landauer formalism) and strongly interacting systems (Lindblad) can control in which drain the current flows. For interacting systems, we find a transition for  $J > \frac{1}{2}$  from a flux-independent to a flux-dependent source current. *By choosing  $\Omega = (2k + 1)/4$ ,  $k$  being integer, we find a non-reciprocal behavior where we can direct the flow into either of the drains.* This could be used as an atomtronic switch to direct the current between different channels, as a transistor or as a rotation sensor.

By sweeping the flux linearly in time, we realize a time-dependent Aharonov-Bohm effect. We find that the current acquires a sinusoidal modulation in time. The frequency of the current is connected to the periodicity of flux  $\Omega \rightarrow \Omega + n$ . *As a result, a constant source current is converted into a alternating current in the drains.* The alternating currents of drain 1 and 2 are shifted relative to each other by a phase  $\pi$ . We can control the frequency

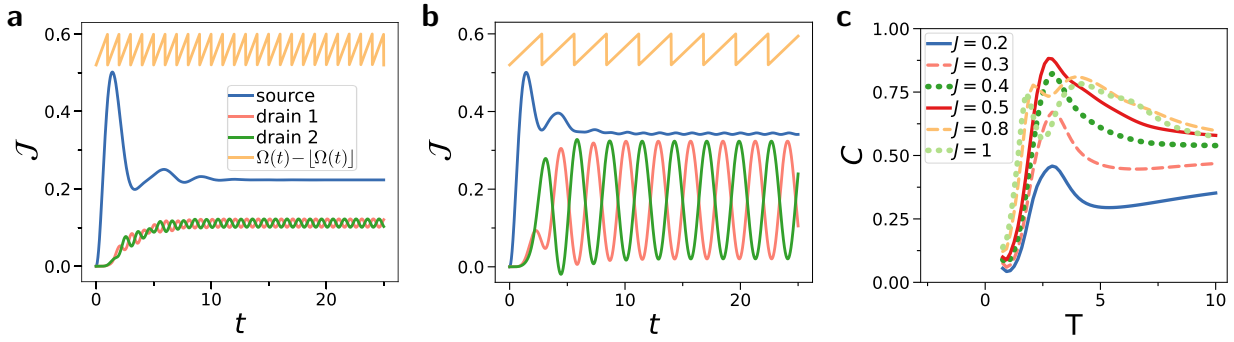


FIG. 5. Current  $\mathcal{J}(t)$  in time  $t$  for various driving periods  $T$  of the flux  $\Omega(t) = t/T$ . **a)**  $T = 1$ , **b)**  $T = 2.8$ . The difference of the flux to the next flux quantum  $\Omega(t) - \lfloor \Omega(t) \rfloor$  is shown in yellow and is not to scale. **c)** DC/AC conversion efficiency  $C = \Delta \mathcal{J}_{\text{drain}} / \langle \mathcal{J}_{\text{source}} \rangle$  measured as the drain current amplitude relative to average source current against driving period  $T$  of the flux  $\Omega(t) = t/T$ . We have  $L = 3$ ,  $K = 1$ ,  $J = 0.5$  and  $B_s = B_d = 1$ .

of the current via the rate change of the flux. We find a near-optimal DC to AC conversion of  $C \approx 0.88$  for  $T = 2.8$  and  $J = 0.5$ . In reverse operation, one can use the system as a sensor for time-dependent rotations  $\Omega(t)$ . By measuring the frequency of the current we can read out how fast the rotation is being accelerated.

The time-dependent synthetic flux allows us to study the time-dependent Aharonov-Bohm effect with cold atoms in a controlled environment, which has been a challenge in other systems [54–57]. We note that the time-dependent synthetic flux lacks the induced electric field of time-dependent magnetic fields. Future studies could simulate the electric field with a time-dependent atomic potential to answer the fundamental open question whether there is a time-dependent Aharonov-Bohm effect for magnetic fields [54–57].

To our knowledge, this is the first cold atom system that exhibits switch-like and frequency generating capabilities. This device is of major interest for experimental cold atom platforms and will help define new applications of Atomtronics.

*Acknowledgements.*— This work is supported by the Singapore Ministry of Education (MOE) and the Singapore National Research Foundation (NRF).

- [3] R. Pepino, J. Cooper, D. Anderson, and M. Holland, Atomtronic circuits of diodes and transistors, *Physical review letters* **103**, 140405 (2009).
- [4] R. Dumke, Z. Lu, J. Close, N. Robins, A. Weis, M. Mukherjee, G. Birk, C. Hufnagel, L. Amico, M. G. Boshier, *et al.*, Roadmap on quantum optical systems, *Journal of Optics* **18**, 093001 (2016).
- [5] L. Amico, G. Birk, M. Boshier, and L.-C. Kwek, Focus on atomtronics-enabled quantum technologies, *New Journal of Physics* **19**, 020201 (2017).
- [6] L. Amico, D. Anderson, M. Boshier, J.-P. Brantut, L.-C. Kwek, A. Minguzzi, and W. von Klitzing, Atomtronic circuits: from basic research in many-body physics to applications for quantum technologies, *arXiv preprint arXiv:2107.08561* (2021).
- [7] A. Pérez-Obiol, J. Polo, and L. Amico, Coherent phase slips in coupled matter-wave circuits, *arXiv preprint arXiv:2112.08072* (2021).
- [8] H. Kiehn, V. P. Singh, and L. Mathey, Implementation of an atomtronic squid in a strongly confined toroidal condensate, *arXiv preprint arXiv:2204.03000* (2022).
- [9] S. Ragole and J. M. Taylor, Interacting atomic interferometry for rotation sensing approaching the heisenberg limit, *Physical Review Letters* **117**, 203002 (2016).
- [10] G. Pelegri, J. Mompart, and V. Ahufinger, Quantum sensing using imbalanced counter-rotating bose-einstein condensate modes, *New Journal of Physics* **20**, 103001 (2018).
- [11] P. Naldesi, J. P. Gomez, V. Dunjko, H. Perrin, M. Olshanii, L. Amico, and A. Minguzzi, Enhancing sensitivity to rotations with quantum solitonic currents, *arXiv preprint arXiv:1901.09398* (2019).
- [12] S. Safaei, L.-C. Kwek, R. Dumke, and L. Amico, Monitoring currents in cold-atom circuis, *Physical Review A* **100**, 013621 (2019).
- [13] E. Arabahmadi, D. Schumayer, M. Edwards, B. Eller, and D. A. Hutchinson, Thermal stability of a quantum rotation sensor, *Physical Review A* **104**, 033323 (2021).
- [14] D. McGloin, G. C. Spalding, H. Melville, W. Sibbett, and K. Dholakia, Applications of spatial light modulators in atom optics, *Optics Express* **11**, 158 (2003).
- [15] C. Ryu and M. G. Boshier, Integrated coherent matter wave circuits, *New Journal of Physics* **17**, 092002 (2015).
- [16] G. Gauthier, I. Lenton, N. M. Parry, M. Baker, M. Davis,

\* [e0032323@u.nus.edu](mailto:e0032323@u.nus.edu)

† On leave from the Dipartimento di Fisica e Astronomia “Ettore Majorana”, University of Catania.

‡ [thaug@ic.ac.uk](mailto:thaug@ic.ac.uk)

- [1] L. Amico, M. Boshier, G. Birk, A. Minguzzi, C. Miniatura, L.-C. Kwek, D. Aghamalyan, V. Ahufinger, D. Anderson, N. Andrei, *et al.*, Roadmap on atomtronics: State of the art and perspective, *AVS Quantum Science* **3**, 039201 (2021).
- [2] B. Seaman, M. Krämer, D. Anderson, and M. Holland, Atomtronics: Ultracold-atom analogs of electronic devices, *Physical Review A* **75**, 023615 (2007).

H. Rubinsztein-Dunlop, and T. Neely, Direct imaging of a digital-micromirror device for configurable microscopic optical potentials, *Optica* **3**, 1136 (2016).

[17] D. Barredo, V. Lienhard, S. De Leseleuc, T. Lahaye, and A. Browaeys, Synthetic three-dimensional atomic structures assembled atom by atom, *Nature* **561**, 79 (2018).

[18] I. Bloch, J. Dalibard, and S. Nascimbene, Quantum simulations with ultracold quantum gases, *Nature Physics* **8**, 267 (2012).

[19] C.-C. Chien, S. Peotta, and M. Di Ventra, Quantum transport in ultracold atoms, *Nature Physics* **11**, 998 (2015).

[20] A. J. Heeger, S. Kivelson, J. Schrieffer, and W.-P. Su, Solitons in conducting polymers, *Reviews of Modern Physics* **60**, 781 (1988).

[21] M. Atala, M. Aidelsburger, J. T. Barreiro, D. Abanin, T. Kitagawa, E. Demler, and I. Bloch, Direct measurement of the zak phase in topological bloch bands, *Nature Physics* **9**, 795 (2013).

[22] H. Miyake, G. A. Siviloglou, C. J. Kennedy, W. C. Burton, and W. Ketterle, Realizing the harper hamiltonian with laser-assisted tunneling in optical lattices, *Physical review letters* **111**, 185302 (2013).

[23] M. Aidelsburger, M. Atala, M. Lohse, J. T. Barreiro, B. Paredes, and I. Bloch, Realization of the hofstadter hamiltonian with ultracold atoms in optical lattices, *Physical review letters* **111**, 185301 (2013).

[24] G. Jotzu, M. Messer, R. Desbuquois, M. Lebrat, T. Uehlinger, D. Greif, and T. Esslinger, Experimental realization of the topological haldane model with ultracold fermions, *Nature* **515**, 237 (2014).

[25] S. C. Caliga, C. J. Straatsma, and D. Z. Anderson, Experimental demonstration of an atomtronic battery, *New Journal of Physics* **19**, 013036 (2017).

[26] J.-P. Brantut, J. Meineke, D. Stadler, S. Krinner, and T. Esslinger, Conduction of ultracold fermions through a mesoscopic channel, *Science* **337**, 1069 (2012).

[27] S. Krinner, D. Stadler, D. Husmann, J.-P. Brantut, and T. Esslinger, Observation of quantized conductance in neutral matter, *Nature* **517**, 64 (2015).

[28] D. Husmann, S. Uchino, S. Krinner, M. Lebrat, T. Gihamachi, T. Esslinger, and J.-P. Brantut, Connecting strongly correlated superfluids by a quantum point contact, *Science* **350**, 1498 (2015).

[29] M. Lebrat, P. Grišins, D. Husmann, S. Häusler, L. Corman, T. Gihamachi, J.-P. Brantut, and T. Esslinger, Band and correlated insulators of cold fermions in a mesoscopic lattice, *Physical Review X* **8**, 011053 (2018).

[30] G. Gauthier, S. S. Szigeti, M. T. Reeves, M. Baker, T. A. Bell, H. Rubinsztein-Dunlop, M. J. Davis, and T. W. Neely, Quantitative acoustic models for superfluid circuits, *Phys. Rev. Lett.* **123**, 260402 (2019).

[31] S. Pandey, H. Mas, G. Drougakis, P. Thekkepatt, V. Bolpasi, G. Vasilakis, K. Poulios, and W. von Klitzing, Hypersonic bose-einstein condensates in accelerator rings, *Nature* **570**, 205 (2019).

[32] T. Haug, L. Amico, R. Dumke, and L.-C. Kwek, Mesoscopic vortex-meissner currents in ring ladders, *Quantum Science and Technology* **3**, 035006 (2018).

[33] T. Haug, R. Dumke, L.-C. Kwek, and L. Amico, Topological pumping in aharonov-bohm rings, *Communications Physics* **2**, 1 (2019).

[34] T. Haug, H. Heimonen, R. Dumke, L.-C. Kwek, and L. Amico, Aharonov-bohm effect in mesoscopic bose-einstein condensates, *Physical Review A* **100**, 041601 (2019).

[35] T. Haug, R. Dumke, L.-C. Kwek, and L. Amico, Andreev-reflection and aharonov-bohm dynamics in atomtronic circuits, *Quantum Science and Technology* **4**, 045001 (2019).

[36] T. F. Haug, *Quantum transport with cold atoms*, Ph.D. thesis, National University of Singapore (Singapore) (2021).

[37] A. Ramanathan, K. Wright, S. R. Muniz, M. Zelan, W. Hill III, C. Lobb, K. Helmerson, W. Phillips, and G. Campbell, Superflow in a toroidal bose-einstein condensate: an atom circuit with a tunable weak link, *Physical review letters* **106**, 130401 (2011).

[38] K. C. Wright, R. Blakestad, C. Lobb, W. Phillips, and G. Campbell, Driving phase slips in a superfluid atom circuit with a rotating weak link, *Physical review letters* **110**, 025302 (2013).

[39] C. Ryu, P. Blackburn, A. Blinova, and M. Boshier, Experimental realization of josephson junctions for an atom squid, *Physical review letters* **111**, 205301 (2013).

[40] B. Eller, O. Oladehin, D. Fogarty, C. Heller, C. W. Clark, and M. Edwards, Producing flow in racetrack atom circuits by stirring, *Physical Review A* **102**, 063324 (2020).

[41] D. Aghamalyan, M. Cominotti, M. Rizzi, D. Rossini, F. Hekking, A. Minguzzi, L.-C. Kwek, and L. Amico, Coherent superposition of current flows in an atomtronic quantum interference device, *New journal of Physics* **17**, 045023 (2015).

[42] T. Haug, J. Tan, M. Theng, R. Dumke, L.-C. Kwek, and L. Amico, Readout of the atomtronic quantum interference device, *Physical Review A* **97**, 013633 (2018).

[43] Y. Aharonov and D. Bohm, Significance of electromagnetic potentials in the quantum theory, *Physical Review* **115**, 485 (1959).

[44] Y. Aharonov and A. Casher, Topological quantum effects for neutral particles, *Physical Review Letters* **53**, 319 (1984).

[45] A. Lobos and A. Aligia, Effects of interactions in transport through aharonov-bohm-casher interferometers, *Physical review letters* **100**, 016803 (2008).

[46] J. Rincón, K. Hallberg, and A. Aligia, Spin-charge separation in strongly interacting finite ladder rings, *Physical Review B* **78**, 125115 (2008).

[47] P. Shmakov, A. Dmitriev, and V. Y. Kachorovskii, Aharonov-bohm conductance of a disordered single-channel quantum ring, *Physical Review B* **87**, 235417 (2013).

[48] S. Olariu and I. I. Popescu, The quantum effects of electromagnetic fluxes, *Reviews of Modern Physics* **57**, 339 (1985).

[49] L. Vaidman, Role of potentials in the aharonov-bohm effect, *Physical Review A* **86**, 040101 (2012).

[50] Y. Gefen, Y. Imry, and M. Y. Azbel, Quantum oscillations and the aharonov-bohm effect for parallel resistors, *Physical review letters* **52**, 129 (1984).

[51] M. Büttiker, Y. Imry, and M. Y. Azbel, Quantum oscillations in one-dimensional normal-metal rings, *Physical Review A* **30**, 1982 (1984).

[52] R. A. Webb, S. Washburn, C. Umbach, and R. Laibowitz, Observation of h e aharonov-bohm oscillations in normal-metal rings, *Physical Review Letters* **54**, 2696 (1985).

[53] Y. Imry, *Introduction to mesoscopic physics*, 2 (Oxford University Press on Demand, 2002).

[54] D. Singleton and E. C. Vagenas, The covariant, time-dependent aharonov–bohm effect, *Physics Letters B* **723**, 241 (2013).

[55] J. Macdougall, D. Singleton, and E. C. Vagenas, Revisiting the marton, simpson, and suddeth experimental confirmation of the aharonov–bohm effect, *Physics Letters A* **379**, 1689 (2015).

[56] J. Jing, Y.-F. Zhang, K. Wang, Z.-W. Long, and S.-H. Dong, On the time-dependent aharonov–bohm effect, *Physics Letters B* **774**, 87 (2017).

[57] S. R. Choudhury and S. Mahajan, Direct calculation of time varying aharonov-bohm effect, *Physics Letters A* **383**, 2467 (2019).

[58] D. Jaksch and P. Zoller, Creation of effective magnetic fields in optical lattices: the hofstadter butterfly for cold neutral atoms, *New Journal of Physics* **5**, 56 (2003).

[59] Y.-J. Lin, R. L. Compton, K. Jiménez-García, J. V. Porto, and I. B. Spielman, Synthetic magnetic fields for ultracold neutral atoms, *Nature* **462**, 628 (2009).

[60] J. Dalibard, F. Gerbier, G. Juzeliūnas, and P. Öhberg, Colloquium: Artificial gauge potentials for neutral atoms, *Reviews of Modern Physics* **83**, 1523 (2011).

[61] T. Haug, R. Dumke, L.-C. Kwek, C. Miniatura, and L. Amico, Machine-learning engineering of quantum currents, *Physical Review Research* **3**, 013034 (2021).

[62] S. Eckel, J. G. Lee, F. Jendrzejewski, N. Murray, C. W. Clark, C. J. Lobb, W. D. Phillips, M. Edwards, and G. K. Campbell, Hysteresis in a quantized superfluid ‘atomtronic’ circuit, *Nature* **506**, 200 (2014).

[63] G. Del Pace, K. Xhani, A. M. Falconi, M. Fedrizzi, N. Grani, D. H. Rajkov, M. Inguscio, F. Scazza, W. Kwon, and G. Roati, Imprinting persistent currents in tunable fermionic rings, arXiv preprint arXiv:2204.06542 (2022).

[64] E. M. Stoudenmire and S. R. White, *ITensor Library (version 2.1.1)*.

[65] H.-P. Breuer, F. Petruccione, *et al.*, *The theory of open quantum systems* (Oxford University Press on Demand, 2002).

[66] C. Guo and D. Poletti, Dissipatively driven hardcore bosons steered by a gauge field, *Physical Review B* **96**, 165409 (2017).

[67] I. Zapata and F. Sols, Andreev reflection in bosonic condensates, *Phys. Rev. Lett.* **102**, 180405 (2009).

[68] A. Daley, P. Zoller, and B. Trauzettel, Andreev-like reflections with cold atoms, *Phys. Rev. Lett.* **100**, 110404 (2008).

[69] R. Landauer, Spatial variation of currents and fields due to localized scatterers in metallic conduction, *IBM Journal of research and development* **1**, 223 (1957).

[70] R. Landauer, Electrical resistance of disordered one-dimensional lattices, *Philosophical magazine* **21**, 863 (1970).

[71] R. Landauer, Electrical transport in open and closed systems, *Zeitschrift für Physik B Condensed Matter* **68**, 217 (1987).

[72] B. Kramer, G. Bergmann, and Y. Bruynseraede, *Localization, Interaction, and Transport Phenomena: Proceedings of the International Conference, August 23–28, 1984 Braunschweig, Fed. Rep. of Germany*, Vol. 61 (Springer Science & Business Media, 2012).

[73] B. Shapiro, Quantum conduction on a cayley tree, *Physical Review Letters* **50**, 747 (1983).

## Appendix A: Landauer formula

The Landauer formula [69–72] is used in mesoscopic systems to express the conductance in terms of the scattering properties of the geometry of the problem. It is a very useful tool to study transport properties and obtain exact expressions for the transport properties of quantum conductors. It has the advantage over semiclassical transport theories that it captures interference phenomena in the conductance. It has been used to calculate the conductance for rings subject to a flux [50, 51]. The formalism expresses branches and junctions in terms of scattering matrices. The geometry of the system we are considering is shown in Fig. 6.

We model the ring as single-channel conductors connecting the branches between the three junctions to the source and drain leads. Each such branch is described as a single scatterer connected to an ideal one-dimensional channel. The scattering can be described with a  $2 \times 2$  scattering matrix

$$\mathcal{S}_j = \begin{bmatrix} r_j & t_j \\ t'_j & r'_j \end{bmatrix}. \quad (\text{A1})$$

All phases and scattering effects that occur within each branch are absorbed into the parameters of the scattering matrix. In the absence of flux through the ring, time-reversal and current-conservation (demanding unitarity) impose the following constraints on the scattering matrix:  $t_j = t'_j$  and  $-t_j/(t'_j)^* = r_j/(r'_j)^*$ . To account for the flux which breaks time-reversal symmetry, we use the Peierls substitution  $t_j \rightarrow t_j e^{-i2\pi\Omega/3}$ ,  $t'_j \rightarrow t_j e^{i2\pi\Omega/3}$ ,  $r_j \rightarrow r_j$ ,  $r'_j \rightarrow r'_j$ . The prior constraints on  $t_j$ ,  $r_j$  and  $r'_j$  remain the same such that we obtain valid scattering matrices. For the  $\mathcal{S}_1$  arm, we get a system of equations that describe the scattering in this arm

$$\begin{bmatrix} B \\ C \end{bmatrix} = \begin{bmatrix} r_1 & t_1 e^{-i2\pi\Omega/3} \\ t_1 e^{i2\pi\Omega/3} & r'_1 \end{bmatrix} \begin{bmatrix} A \\ D \end{bmatrix}. \quad (\text{A2})$$

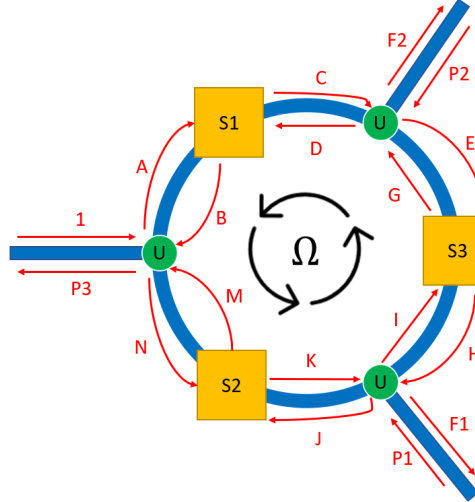


FIG. 6. Three-terminal ring device described with Landauer formula. The left channel represents the path towards the source lead, while the top and bottom right channels represent the path towards the two drains. The arms of the ring are represented by scattering matrices  $S_1$ ,  $S_2$  and  $S_3$ , and the flux is absorbed into their parameters via the Peierls substitution. The junctions connecting ring to source and drains are represented by the scattering matrix  $\mathcal{U}$ .

We can model the junctions that connect to the leads with a  $3 \times 3$  scattering matrix  $\mathcal{U}$  [73]:

$$\mathcal{U} = \begin{bmatrix} 0 & -\frac{1}{\sqrt{2}} & -\frac{1}{\sqrt{2}} \\ -\frac{1}{\sqrt{2}} & \frac{1}{2} & -\frac{1}{2} \\ -\frac{1}{\sqrt{2}} & -\frac{1}{2} & \frac{1}{2} \end{bmatrix}. \quad (\text{A3})$$

The first channel is the path leading out of the ring to one of the leads.  $\mathcal{U}$  describes a scenario where there is no instantaneous reflection for particles entering the ring from the channel and we can scatter in both directions in the ring with equal probability. While the scattering matrix  $\mathcal{U}$  that fulfils these conditions is not unique, the results do not qualitatively depend on the specific choice of  $\mathcal{U}$ .

We solve the equations by writing down the relationships between the various amplitudes at the junctions and scatterers. We demand that the channel of the source lead into the ring is unitary and setting that  $P_1$  and  $P_2$  is zero, which means that particles that exit to the drains cannot return. As a result, we get a linear system of 15 equations and 15 unknowns. We solve it for  $F_1$  and  $F_2$  which are the complex amplitudes of the transmission into the respective drains. Then, we insert the values for all the scattering coefficients  $t_j$ ,  $r_j$  and  $r'_j$ .

The final result depends on how we choose these scattering coefficients as they determine the transport properties of the ring. From physical consideration, we demand that transmission and reflection occur with equal probability and we demand that clockwise and anti-clockwise reflection is the same  $r_j = r'_j$ . These consideration lead us to the choice  $r_j = r'_j = \sqrt{1/2}$  and  $t_j = i\sqrt{1/2}$ .

The transmission  $T_\alpha = |F_\alpha|^2$  into the respective drains  $\alpha \in \{0, 1\}$  is given by

$$F_\alpha = 16 \left| \frac{1 - \sqrt{2} + 2i(2\sqrt{2} - 3) \exp(-i\pi(2\Omega + \alpha))}{62 - 46\sqrt{2} + 2i \cos(\pi(2\Omega + \alpha))} \right|^2 \quad (\text{A4})$$

As seen in the main text, the transmission strongly depends on the flux  $\Omega$  and can be tuned to maximize transmission into a particular drain.

## Appendix B: Flux dependence of dynamics close to ground state

Here, we show the change in density for the three terminal device close to the ground state. We prepare a density perturbation in the source, then quench the Hamiltonian and create a propagating density wave. The dynamics for different values of flux is shown in Fig.7. Note that  $\Omega = 0.25 + k$  and  $\Omega = 0.75 + k$  produces nearly the same dynamics.

For any value of flux, we observe that the current into drain 1 and drain 2 is nearly identical. We also find a reflection symmetry  $\Omega \rightarrow -\Omega$  for the dynamics close to the ground state. Both the reflection symmetry and the symmetry in the drain is absent for the strongly perturbed dynamics.

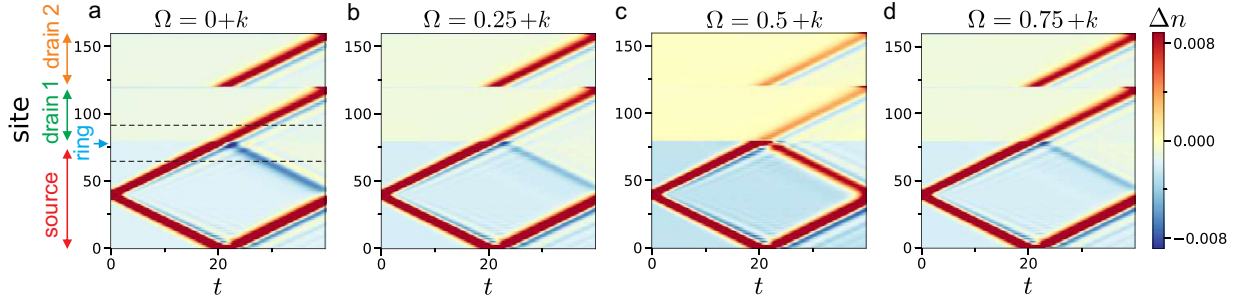


FIG. 7. Dynamics of density wave in three-terminal device. **a)** Change of density relative to average density  $\Delta n(t) = \langle n(t) \rangle - n_0$  as function of time and sites of source, ring, drain 1 and 2. We show **a)**  $\Omega = k$  **b)**  $\Omega = 0.25 + k$ , **c)**  $\Omega = 0.5 + k$  and **d)**  $\Omega = 0.75 + k$ , where  $k$  is an integer. Perturbation starts in source, and moves through ring into drains. Note that the dynamics in both drains is symmetric for all values of flux.

### Appendix C: Time-dependent flux

For very slow driving  $T \gg 1$ , the system dynamics is much faster than the driving. Thus, the system has sufficient time to settle into the instantaneous steady state of the flux. The current then simply follows the current of the steady state of the system  $\rho_{\text{ss}}(\Omega(t))$ . We show the dynamics in this case in Fig. 7

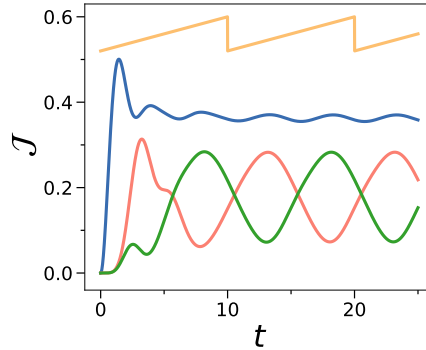


FIG. 8. Current  $J(t)$  in time  $t$  for various driving periods  $T$  of the flux  $\Omega(t) = t/T$  for  $T = 10$ . The difference of the flux to the next flux quantum  $\Omega(t) - \lfloor \Omega(t) \rfloor$  is shown in yellow and is not to scale. We have  $L = 3$ ,  $K = 1$ ,  $J = 0.5$  and  $B_s = B_d = 1$ .

### Appendix D: Experimental details

Here we give details on the experimental demonstration of the Bose-Einstein condensate in the potential of a three-terminal ring in Fig. 1b. The experiment starts with a Magneto-Optical Trap (MOT) which traps up to  $7 \times 10^8$  Rubidium 87 atoms down to temperatures of  $20\mu\text{K}$  for 5ms. Magnetic field biases with an optical pump beam pumps the atoms into the  $F = 2, m_f = +2$  state. A magnetic field gradient of  $220\text{G/cm}$  is then ramped up in 150ms to trap up to  $3 \times 10^8$  atoms. A 2 second translation stage brings the atoms to a second magnetic trap with lower vacuum pressure. Due to heating processes during this step, a Radio-Frequency (RF) evaporative cooling step is then further performed to condense the atoms back to  $20\mu\text{K}$ . An atom cloud of  $1 \times 10^7$  atoms remains after this step. At the same time, a 1064nm laser beam for optical trapping of the atoms is ramped up to 5W, and subsequently a ramp down of the MOT is performed, leaving behind a pure optical trap.

Next, an optical evaporation step is performed. The laser power is first lowered from 9.0V to 6.0V in 2s, where the atom temperature reaches  $1\mu K$  and the atom number is  $1 \times 10^6$ . The second ramp brings the voltage from 6.0V to 5.0V in 3s with a temperature of 250nK and atom number  $3.5 \times 10^5$ .

The final ramp occurs in 2s from 5.0V to 4.8V where we get a Bose-Einstein condensate (BEC) of  $1.8 \times 10^5$  atoms with a phase space density of 3.0. The optical setup for creating arbitrary traps in 2D comprises a Digital Micromirror Device (DMD) setup and an optical sheet. The DMD (DLP9500) has dimensions of 20.7mm x 11.7mm with pitch of  $10.8\mu m$ . A controller board (V4395) from Texas Instruments controls the operation of the DMD. A blue-detuned (532nm) 10mm beam diameter is reflected off the DMD with 40% efficiency in the first order with all mirrors on. This beam is first de-magnified 4 times with a 300mm-75mm lens configuration, and later 20 times with a 200mm-20x objective (Mitutoyo M Plan APO NIR 20x, NA = 0.40) for a total of 80x de-magnification. The 1st order beam at the atom plane has a maximum 190mW of beam power at a beam radius of  $62.5\mu m(1/e^2)$  giving a maximum trap depth of  $1.8\mu K$ . Utilising the same objective lens, a dichroic mirror reflects the absorption image of the atoms through a 200mm lens and imaged onto an ANDOR EMCCD. The resonant imaging beam is delivered from below the atoms with a pulse time of 10 $\mu s$  to minimise the force on the atoms. The optical sheet for 2D trapping is generated via intersecting 2 beams using a single lens. The interference of the 2 beams creates optical sheets superimposed on the beam profile. Our beam is asymmetric at the focus with 50 $\mu m$  radius in the vertical direction and 150  $\mu m$  in the horizontal direction. This minimises the probability of loading into multiple sheets as the interfering beams are static. The interfering beams are distanced such that the interference sheets are spaced 7.5 $\mu m$  apart.

Loading of a BEC into the combined blue-detuned trap starts with a BEC at 50% purity in the red-detuned crossed dipole trap. The desired trap is first projected on the DMD, and within 100ms both the DMD and optical sheet are ramped up while keeping the red-detuned trap on. The DMD beam is ramped up to half power while the sheet is ramped up to 63mW per interfering beam. The red-detuned trap is ramped down to a negligible trap depth in 10ms to complete the transfer. The transfer efficiency of the atoms heavily depends on the size of the DMD trap as compared to the initial BEC size. A DMD square trap of side 40 $\mu m$  gives a loading efficiency of 50%. The condensation of the BEC in the DMD is verified by observing in the time-of-flight images an asymmetric cloud in the direction perpendicular to the sheet.